Quasi-Lagrangian superpressure balloon measurements of gravity-wave momentum fluxes in the polar stratosphere of both hemispheres

R. A. Vincent,[1] A. Hertzog,[2] G. Boccara,[2] and F. Vial[2]

Received 21 June 2007; revised 15 August 2007; accepted 4 September 2007; published 3 October 2007.

[1] Superpressure balloons were flown in 2002 and 2005 in the winter polar vortices of both hemispheres. The balloons can drift for months in the stratosphere acting as quasi-Lagrangian tracers of air-parcel motions. The meteorological datasets acquired are used to retrieve small-scale internal atmospheric gravity wave parameters using wavelet techniques. For the first time, gravity wave momentum fluxes are estimated over wide geographical areas and the results will help constrain gravity wave parameterization schemes used in general circulation climate models. The importance of mountain waves is confirmed, with largest fluxes observed in the lee of Greenland and the Antarctic Peninsula. However, significant momentum fluxes are also observed over the oceans, showing the importance of other wave generation mechanisms. **Citation:** Vincent, R. A., A. Hertzog, G. Boccara, and F. Vial (2007), Quasi-Lagrangian superpressure balloon measurements of gravity-wave momentum fluxes in the polar stratosphere of both hemispheres, *Geophys. Res. Lett.*, *34*, L19804, doi:10.1029/2007GL031072.

1. Introduction

[2] Internal atmospheric inertia-gravity (buoyancy) waves efficiently transfer energy and momentum from source regions in the lower atmosphere to the upper atmosphere and play a role in determining the state of the atmosphere and climate. The decrease of atmospheric density with height produces an exponential growth of wave amplitudes, leading to wave breaking and dissipation. At the solstices the resulting momentum transfer to the mean flow drives a pole-to-pole meridional circulation that profoundly affects the chemical composition and the thermal structure of the middle atmosphere [e.g., *Holton et al.*, 1995]. Gravity waves (GW) are also linked to the formation of polar stratospheric clouds and the associated microphysical processes that play a crucial role in ozone destruction [*Eckermann and Preusse*, 1999; *Höpfner et al.*, 2006]. GW are generated over a wide range of temporal and spatial scales by a variety of sources, including flow over mountains, convection, flow adjustment and wind shear [*Fritts and Alexander*, 2003]. Accounting for GW effects in global atmospheric circulation models (GCM) requires understanding of geographical and temporal variability, generation mechanisms and resulting wave characteristics.

[3] GW effects are usually parameterized in models since explicit simulation of a full 3-dimensional wave spectrum and its evolution with altitude is computationally intensive. A variety of parameterization schemes have been proposed that involve a description of the distribution of momentum flux as a function of ground-based phase speed or its equivalent [*Hines*, 1997; *Alexander and Dunkerton*, 1999; *Warner and McIntyre*, 2001]. Such schemes suffer from a lack of observational constraints. The wide variety of tunable parameters means that a model tuned for one set of parameters cannot be used in any prognostic manner [*Charron et al.*, 2002].

[4] Information on GW momentum fluxes on a global basis is difficult to obtain. A variety of techniques that use large ground-based radars, radiosondes and satellite limb sounding or radio-occultation methods have been used [e.g., *Eckermann and Preusse*, 1999; *Tsuda et al.*, 2000; *Ern et al.*, 2004], but suffer from either poor geographic coverage or require a number of assumptions that cannot easily be tested. Ground and space-based techniques are usually unable to measure the wave intrinsic frequency (the frequency measured in a reference frame moving with the background wind), which determines important wave properties [*Gossard and Hooke*, 1975].

[5] Measurements made with balloons that drift quasi-horizontally with the background wind do not suffer this limitation. The use of superpressure balloons (SPB) to study GW was pioneered by *Massman* [1981] who analyzed data acquired in the southern hemisphere during the Tropical Wind, Energy Conversion and Reference Level Experiment (TWERLE). At the float level, the gas inside the closed envelope of a SPB is kept at a pressure greater than that of the ambient atmospheric pressure. The balloon always remains spherical during flight and experiences vertical displacements of less than 20 m at sunrise/sunset so it is advected by the horizontal wind on a constant density surface. Here we present recent ultra-long-duration SPB observations that provide measurements of wave fluxes over wide geographical areas in the lower stratosphere of the polar regions of both hemispheres.

2. Observations

[6] The balloons used in this study were developed by the French Space Agency (CNES) in the framework of the Stratéole-Vorcore project. Balloons of 8.5-m and 10-m diameter float at respective altitudes of about 17 and 19 km, equivalent to pressure levels of $p_o \sim 75$ hPa and $p_o \sim 55$ hPa in the polar wintertime stratosphere. Six SPB test flights were launched from Kiruna (68°N, 20°E) in the Arctic in early February 2002. The longest flight duration achieved during this campaign was 45 days, with most of

[1]Department of Physics, University of Adelaide, Adelaide, South Australia, Australia.
[2]Laboratoire de Météorologie Dynamique, École Polytechnique, Palaiseau, France.

0094-8276/07/2007GL031072$05.00

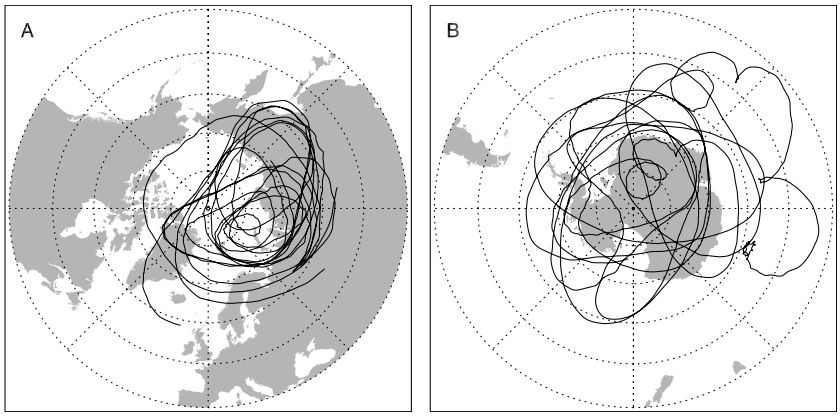

Figure 1. (a) Trajectories of SPB launched from Kiruna in early February 2002. The last flight terminated on March 21. (b) Trajectory of Vorcore SPB-11 (8.5-m diameter) launched on 23 September 2005 from McMurdo. The flight terminated on 26 December.

the flights automatically cut-down when crossing 55°N (a limit imposed so as to avoid flying over populated areas). During the Vorcore campaign, 27 SPB were released from McMurdo, Antarctica (78°S, 167°E) between September 5 and October 28, 2005. The longest Vorcore flight lasted 109 days and the mean flight duration during the campaign was about 59 days [*Hertzog et al.*, 2007].

[7] Each balloon carried a light gondola to perform scientific observations and to monitor the balloon flight safety. Air temperature and pressure were recorded every 15 min with an accuracy, respectively, of 0.3 K and 1 Pa, the latter value corresponding to vertical displacements of about 1 m. Global Positioning System (GPS) measurements were used to determine balloon location with an accuracy of 10 m in the horizontal and 20 m in the vertical. Zonal and meridional wind speeds along the flight track were obtained by finite differencing of successive 15-min GPS positions to an accuracy of better than 0.1 ms^{-1}. Data were uploaded to the ARGOS satellite system for transmission to ground stations, with the ARGOS bandwidth determining the effective sampling rate.

[8] The results presented in this article were obtained from five flights in the Kiruna 2002 campaign and one from the McMurdo 2005 campaign, in order to have about the same number of observation days in both case studies. Trajectories of these flights are shown in Figure 1. All Arctic flights occurred within the polar stratospheric vortex, as well as the major part of the Antarctic flight. This means that orographic (zero phase speed) waves were still able to penetrate into the Antarctic stratosphere and so the seasonal discrepancy between the northern and southern flights is compensated for by the longer duration of the SH vortex.

3. Data Analysis

3.1. Estimation of Momentum Flux

[9] As a SPB drifts under the influence of the background wind it experiences perturbations in velocity, pressure and temperature induced by inertia gravity waves. One problem with the present SPB system is that the relatively poor accuracy of the vertical position measurements precludes direct calculation of the vertical velocity and hence a direct estimate of the flux of momentum. Instead we use the cross-spectrum between the pressure and horizontal velocity, which can be related to the momentum flux with the assumption that there are only upward-propagating waves in the lower stratosphere.

[10] Analysis of the SPB data starts by noting that GW horizontal velocity perturbations are elliptically polarized, with the major axis of the ellipse aligned along the horizontal direction of propagation [*Gossard and Hooke*, 1975]. Furthermore, the GW pressure perturbation p' is due to two components. The first (Eulerian) component is the pressure disturbance induced directly by the wave. The second (Lagrangian) component is caused by the vertical motion in the presence of the background pressure gradient. These two components are in quadrature and both are proportional to $u'_{\|}$, the horizontal perturbation velocity aligned with the major axis of the perturbation ellipse. *Hertzog and Vial* [2001] describe in more detail how the momentum flux is derived from the pressure and horizontal velocity components.

3.2. Wavelet Analysis

[11] In practice, the measured fluctuations are caused by the superposition of a wide spectrum of gravity wave packets generated by different sources and propagating in different directions. Wavelet analysis is well suited for extracting the fluxes from the time series of the horizontal velocity and pressure since it decomposes data as a function of intrinsic-period (frequency) and time (space) [*Torrence and Compo*, 1998; *Zink and Vincent*, 2001]. Here, the complex Morlet wavelet, which has a Gaussian envelope, was used for its packet-like qualities.

[12] Let $\tilde{p}$, $\tilde{u}$ and $\tilde{v}$ be the respective wavelet transforms of pressure, zonal and meridional velocity. A first selection is performed among the wavelet coefficients to retain only those that pass several criteria, including signal-to-noise ratios larger than a predetermined threshold and intrinsic periods ranging from 1 hour to the local inertial period.

[13] The wave directions of propagation are then found by rotating the horizontal axes of the polarization ellipse and maximizing the ratio of parallel $\tilde{u}_{\|}$ to perpendicular $\tilde{u}_{\perp}$

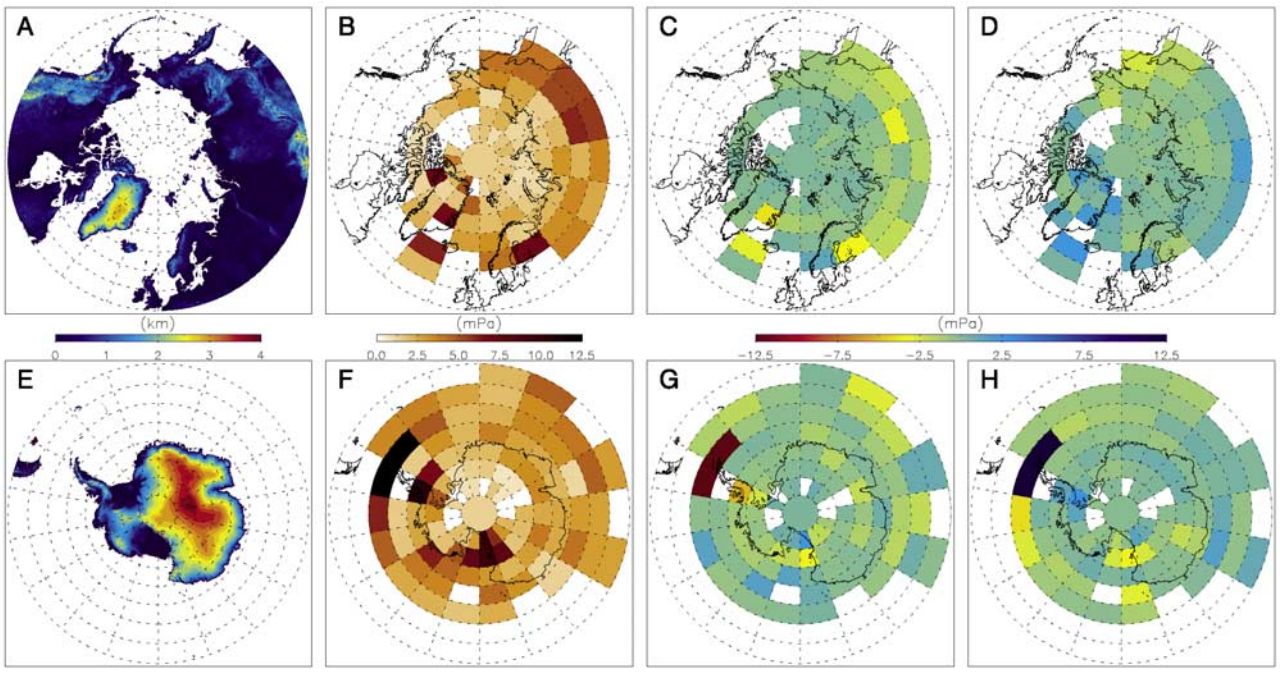

Figure 2. (a) Topography in km of the high-latitude Northern Hemisphere. (b) Geographic distribution of density-weighted momentum fluxes in the propagation direction of the waves. (c) Density-weighted zonal and (d) meridional momentum fluxes for the Arctic. (e, f, g, h) Same as for Figure s 2a–2d, but for the high-latitude Southern Hemisphere. Bins with less than 20 observations are left blank in the momentum maps.

(aligned with the ellipse minor axis) velocity fluctuations. The local contribution to the momentum flux is then

$$\tilde{u}_{\|}\tilde{w}^{*} = \frac{\hat{\omega}g}{p_o N^2}\mathcal{I}\left(\tilde{p}\tilde{u}_{\|}^{*}\right). \quad (1)$$

where $\hat{\omega}$ is the intrinsic frequency, g is the acceleration due to gravity, p_o the pressure at the float level, N is the buoyancy frequency, $\mathcal{I}$ signifies imaginary part, and the asterisk denotes the complex conjugate.

[14] Lastly, the mean momentum flux along the flight $\overline{u'_{\|}w'}$ is recovered by summing the selected individual contributions according to the wavelet Parseval's theorem [*Torrence and Compo*, 1998]. The same procedure is followed to obtain the mean zonal and meridional components, except that the individual contributions of total momentum flux are first projected on the zonal and meridional directions.

3.3. Numerical Simulations

[15] A large number of Monte-Carlo type simulations were performed to test the technique and understand its limitations and uncertainties. Time series were generated by "flying" balloons through a model that mimicked the observations with realistic noise and sampling rates. Each series contained one or more wave packets that were allowed to "propagate" in the model. Wave characteristics, such as direction, phase speed and period, were randomly assigned; the only restrictions were that each packet consisted of at least two oscillations and that the amplitude was small enough to preclude wave instabilities. The amplitudes were chosen so that they satisfied observations that show an approximate $\hat{\omega}^{-2}$ spectral distribution [*Hertzog and Vial*, 2001].

[16] It is found from simulations with a single gravity-wave packet in each time series that wave directions of propagation are almost perfectly retrieved. Due to the selection performed among the wavelet coefficients, the momentum flux tends to be underestimated on average by about 10% with an uncertainty of about 10%, which is still an order of magnitude better than space-borne estimations [*Ern et al.*, 2004]. The 15-min data rate results in undersampling of the highest-frequency waves (periods $\sim$ 1 hr), and produces poor momentum-flux retrievals for those waves.

[17] In practice, however, several wave packets are likely to be present simultaneously, and so time series with either two or ten wave packets were used to evaluate the consequences for the retrieval of wave parameters. In these situations the relations between velocity and pressure wavelet coefficients are modified when wave packets locally overlap in time-frequency space. The analysis tends to discard those coefficients, which leads to further underestimation of momentum fluxes. Typically, 80% of the input momentum flux is retrieved in the 10-wave time series, while the uncertainty is unchanged ($\sim$10%).

4. Results

[18] The retrieved momentum fluxes can be decomposed in a variety of ways, as shown in Figure 2. The geographical decompositions of the density-weighted momentum fluxes in the wave propagation direction appear in Figures 2b and 2f in $5^\circ \times 20^\circ$ latitude-longitude bins (except around the pole). In the northern hemisphere (NH), the geographical variabil-

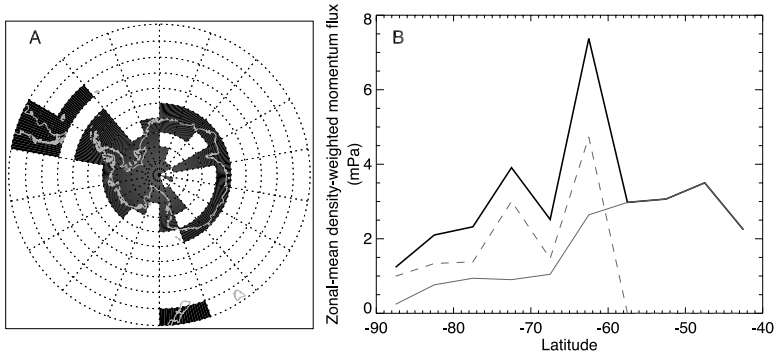

Figure 3. (a) Geographical bins assumed to generate only orographic waves (either classical lee waves or waves generated by katabatic flow) (black), and only non-orographic waves (most likely jet and adjustment processes at sub-polar latitudes) (white). (b) Zonal-mean density-weighted momentum fluxes in the propagation direction of the wave ($\rho_o \overline{u'_{||} w'}$) produced by orographic waves (gray dashed), and non-orographic waves (gray solid). The sum of both fluxes (the zonal-mean total flux) is shown with the black solid curve. The fluxes are plotted at the mean latitude of each latitudinal band.

ity is dominated by large fluxes near mountainous regions (Figures 2a and 2b) such as along the edges of Greenland, the Scandinavian Peninsula and Eastern Siberia. In the southern hemisphere (SH) the most active areas are found in the vicinity of the Antarctic Peninsula and the Trans-antarctic mountains (Figures 2e and 2f), which agrees with satellite observations of wave-induced temperature disturbances [*Wu and Jiang*, 2002; *Jiang et al.*, 2004; *Wu and Eckermann*, 2007]. However, significant momentum flux is also observed in oceanic regions and is thus associated with non-orographic gravity-wave sources. The magnitude of the fluxes are clearly different in both hemispheres, with mean values of 3.4 mPa observed in the southern hemisphere compared with 2.6 mPa in the northern hemisphere. This is mostly caused by the momentum fluxes observed above the Antarctic Peninsula that exceed by a factor of 2 the momentum fluxes in every other sampled region. However, this hemispheric contrast may require further confirmation since the NH was not sampled as homogeneously as the SH. In particular, no observations were made in the western hemisphere and therefore potentially significant GW sources were missed, such as the Alaskan Brooks Range.

[19] Figures 2c and 2g display the density-weighted zonal momentum fluxes. Strikingly, the zonal momentum flux is negative almost everywhere, which indicates that the vast majority of GW are propagating against the mean eastward flow characteristic of the wintertime stratosphere. The largest westward fluxes are found above or in the lee of major orography, and locally reach 12 mPa over the Antarctic Peninsula. Note that the flux in a given region is both a spatial and temporal average of all the balloon passages in this region (as are all values reported in this article) and may cover both mountainous and oceanic surfaces. Much stronger individual wave packets that had fluxes 50 times larger than the average were locally observed directly above the Peninsula, as also reported from the ER-2 aircraft measurements of *Bacmeister et al.* [1990]. Away from the mountains, the average zonal fluxes are typically smaller than 3 mPa.

[20] The meridional momentum fluxes are displayed in Figures 2d and 2h. In contrast to the zonal momentum fluxes, they are generally smaller in magnitude and both positive and negative values are observed, respectively associated with northward- and southward-propagating waves. The NH values are uniformly small. In the SH significant positive values ($\sim$10 mPa) are observed in the vicinity of the Antarctic Peninsula (likely associated with the main orientation of the ridges), whereas negative values with smaller magnitudes ($\sim$3 mPa) are generally found above the southern oceans.

[21] A simple geographical criterion is used to distinguish between the relative role of orographic and non-orographic GW momentum fluxes in the SH. Waves observed above areas with steep topography and in their direct lee are assumed to be generated by mountain processes, including waves produced by katabatic winds. The algorithm used to flag the "orographic" areas is as follows: starting from the NOAA 5″ x 5″ gridded elevation dataset the gradient of elevation was computed at the same resolution. The mean of the 10% largest gradients were then calculated for each latitude-longitude bin. The bins for which the mean exceeds a (conservative) threshold value of 15 m km^{-1} were flagged as orographic. A few areas located directly in the lee of major orography (such those to the east of the Antarctic Peninsula) were also included. All waves observed elsewhere are assumed to have a non-orographic origin, probably adjustment, frontal and jet processes at the latitudes considered. Figure 3a displays the areas that are assumed to generate mountain waves. Note in particular the asymmetry between the mountainous West Antarctica and the smoother East Antarctica.

[22] The result of this partition of momentum is displayed in Figure 3b. Orographic waves carry about 2/3 of the total momentum flux above Antarctica. Our results therefore confirm the predominance of wave activity over western Antarctica, which has been invoked as a potential factor to explain the PSC asymmetry above the continent [*Höpfner et al.*, 2006]. The largest values of zonal-mean momentum flux associated with orographic waves are observed at latitudes that correspond to the Peninsula. It should be emphasized, however, that the relative decrease of orographic momentum flux between 65°S and 70°S should not be misinterpreted as it may result from the absence of observations in that latitudinal band over the Peninsula.

[23] On the other hand, the momentum flux associated with non-orographic waves shows two distinct patterns,

with small values at the highest latitudes, and an abrupt increase north of 65°S. Zonal-mean values of 3 mPa are observed above the Southern Ocean. These oceanic values are strikingly similar to the fluxes produced by orographic waves at the edge of Antarctica and therefore emphasize the importance of non-orographic gravity waves in the global transport of momentum. The mechanism(s) that generates these waves is uncertain, but the predominance of their observation above the oceans obviously means that they have a non orographic origin. Although further confirmation is needed, adjustment of tropospheric disturbances toward geostrophic balance may explain the enhanced observation of GW fluxes at latitudes corresponding to the tropospheric storm tracks [*O'Sullivan and Dunkerton*, 1995]. Future work will examine the relationship between wave fluxes and sources.

[24] **Acknowledgments.** The support of CNES and CNRS/INSU is gratefully acknowledged. The project also benefited from the help of IPEV and from NSF. The Vorcore technological and operational success resulted from the collaboration between the CNES balloon subdirectorate and LMD. RAV acknowledges travel support from the Scientific Visits to Europe Scheme of the Australian Academy of Science and Department of Science and Environment.

References

Alexander, M. J., and T. J. Dunkerton (1999), A spectral parameterization of mean-flow forcing due to breaking gravity waves, *J. Atmos. Sci.*, *56*, 4167–4182.

Bacmeister, J. T., M. R. Schoeberl, L. R. Lait, P. A. Newman, and B. Gary (1990), ER-2 mountain wave encounter over Antarctica: Evidence for blocking, *Geophys. Res. Lett.*, *17*, 81–84.

Charron, M., E. Manzini, and C. D. Warner (2002), Intercomparison of gravity wave parameterizations: Hines doppler-spread and Warner and McIntyre ultra-simple schemes, *J. Meteorol. Soc. Jpn.*, *80*, 335–345.

Eckermann, S. D., and P. Preusse (1999), Global measurements of stratospheric mountain waves from space, *Science*, *286*, 1534–1537.

Ern, M., P. Preusse, M. J. Alexander, and C. D. Warner (2004), Absolute values of gravity wave momentum flux derived from satellite data, *J. Geophys. Res.*, *109*, D20103, doi:10.1029/2004JD004752.

Fritts, D. C., and M. J. Alexander (2003), Gravity wave dynamics and effects in the middle atmosphere, *Rev. Geophys.*, *41*(1), 1003, doi:10.1029/2001RG000106.

Gossard, E. E., and W. H. Hooke (1975), *Waves in the Atmosphere*, Elsevier, New York.

Hertzog, A., and F. Vial (2001), A study of the dynamics of the equatorial lower atmosphere by use of ultra-long-duration balloons: 2. Gravity waves, *J. Geophys. Res.*, *106*, 22,745–22,761.

Hertzog, A., et al. (2007), Stratéole/Vorcore long-duration, superpressure balloons to study the Antarctic lower stratosphere during the 2005 winter, *J. Atmos. Oceanic Technol.*, in press.

Hines, C. O. (1997), Doppler-spread parameterization of gravity-wave momentum deposition in the middle atmosphere. Part 1: Basic formulation, *J. Atmos. Sol. Terr. Phys.*, *59*, 371–386.

Holton, J. R., P. H. Haynes, M. E. McIntyre, A. R. Douglass, R. B. Rood, and L. Pfister (1995), Stratosphere-troposphere exchange, *Rev. Geophys*, *33*, 403–439.

Höpfner, M., et al. (2006), MIPAS detects Antarctic stratospheric belt of NAT PSCs cause by mountain waves, *Atmos. Chem. Phys.*, *6*, 1221–1230.

Jiang, J. H., S. D. Eckermann, D. L. Wu, and J. Ma (2004), A search for mountain waves in MLS stratospheric limb radiances from the winter Northern Hemsiphere: Data analysis and global mountain wave modeling, *J. Geophys. Res.*, *109*, D03107, doi:10.1029/2003JD003974.

Massman, W. J. (1981), An investigation of gravity waves on a global scale using TWERLE data, *J. Geophys. Res.*, *86*, 4072–4082.

O'Sullivan, D., and T. J. Dunkerton (1995), Generation of inertia-gravity waves in a simulated life-cycle of baroclinic instability, *J. Atmos. Sci.*, *52*, 3695–3716.

Torrence, C., and G. P. Compo (1998), A practical guide to wavelet analysis, *Bull. Am. Meteorol. Soc.*, *79*, 61–78.

Tsuda, T., M. Nishida, C. Rocken, and R. Ware (2000), Global morphology of gravity wave activity in the stratosphere revealed by the GPS occultation data (GPS/MET), *J. Geophys. Res.*, *105*, 7257–7274.

Warner, C. D., and M. E. McIntyre (2001), An ultrasimple spectral parameterization for nonorographic gravity waves, *J. Atmos. Sci.*, *58*, 1837–1857.

Wu, D. L., and S. D. Eckermann (2007), Global gravity wave variances from AURA MLS: Characteristics and interpretation, *J. Atmos. Sci*, in press.

Wu, D. L., and J. H. Jiang (2002), MLS observations of atmospheric gravity waves over Antarctica, *J. Geophys. Res.*, *107*(D24), 4773, doi:10.1029/2002JD002390.

Zink, F., and R. A. Vincent (2001), Wavelet analysis of stratospheric gravity wave packets over Macquarie Island: 1. Wave parameters, *J. Geophys. Res.*, *106*, 10,275–10,287.

R. A. Vincent, Department of Physics, University of Adelaide, Adelaide SA 5005, Australia. (robert.vincent@adelaide.edu.au)

G. Boccara, A. Hertzog, and F. Vial, Laboratoire de Météorologie Dynamique, École Polytechnique, F-91128 Palaiseau Cedex, France. (gillian.boccara@lmd.polytechnique.fr; hertzog@lmd.polytechnique.fr; vial@lmd.polytechnique.fr)